Differential GPS Reference Station Algorithm—Design and Analysis

Jay Farrell, *Senior Member, IEEE* and Tony Givargis

***Abstract*—The global positioning system (GPS) allows properly equipped users to determine their position based on the measured pseudoranges to at least four satellites. Differential GPS operation (DGPS) uses a reference station at a known location to calculate and broadcast pseudorange corrections to local users, resulting in improved user position accuracy. DGPS accuracy is limited by the ability of the reference station to remove the effects of receiver measurement noise and multipath errors from the broadcast corrections. This article presents two new algorithms for DGPS reference station design. The accuracy of the algorithms is analyzed both theoretically and experimentally. The single and two frequency reference station algorithms, respectively, achieve 6 dB and >20 dB improvement relative to the raw corrections.**

***Index Terms*—Differential global positioning, global positioning system, Kalman filtering, multipath channels, navigation, state estimation.**

I. Introduction

THE GLOBAL positioning system (GPS) allows properly equipped users to determine their position based on the measured pseudoranges to at least four satellites. Discussion of GPS terminology and positioning algorithms can be found, for example, in [4], [9], and [12]. GPS positioning accuracy is limited by measurement errors that can be classified as either common mode or noncommon mode. Common mode errors have nearly identical effects on all receivers operating in a limited geographic area (<50 km). Noncommon mode errors are distinct even for two receivers with minimal antenna separation. The common mode pseudorange errors have a typical standard deviation on the order of 25 m for civilian receivers. The common mode errors are smooth, continuous signals with correlation times on the order of 300 s. The noncommon mode errors are dominated by multipath and receiver noise.

A basic understanding of the operation of a GPS receiver will help to understand the corrupting effects of multipath. The receiver determines the GPS signal transit time by correlating an internally generated version of a pseudorandom code with the received satellite signal. The internally generated signal is shifted in time until maximum correlation occurs. The time shift, relative to the known time at which the satellite generated the signal, corresponding to maximum correlation between the two signals is the measured transit time. Ideally, the correlation envelope is symmetric about its maximum value. This symmetry simplifies the process of determining the peak correlation time shift.

Multipath errors are due to reflected signals from surfaces along the direct signal path from the satellite to the receiver. The reflected signals shift the correlation peak and corrupt the theoretically symmetric receiver correlation envelope. Both of these changes to the correlation envelope result in erroneous pseudorange measurements. Multipath errors affect both stationary and mobile receivers. For mobile receivers, the signal path and reflecting geometries are changing, so the correlation time of multipath errors for roving receivers is significantly smaller than for stationary receivers. In both stationary and mobile applications, the unknown characteristics of the direct and reflected signal paths make modeling (and prediction) of the multipath errors an infeasible task.

Code multipath can result in pseudo-range errors of 0.1–3.0 m depending on various design and antenna siting factors (e.g., correlator and choke ring technology, antenna height). The theoretical results presented later cover this entire range of multipath signal levels. L1 phase multipath error is less than 5 cm. Receiver measurement noise is predominantly high frequency and has a standard deviation between 0.2–1.5 m depending on receiver technology.

GPS or GPS aided inertial navigation systems (INS) are candidate navigation systems for vehicle control applications in farming, aviation, rail, marine, mining, and dredging [1], [10]. For most control applications, the ≈100 m. standard GPS accuracy is not sufficient. Differential GPS (DGPS) techniques can produce positioning accuracies at the 1–10 m level. These accuracies are sufficient to enable new automated vehicle control applications. The present article presents and analyzes new algorithms for implementation of the DGPS *reference station* based on optimal filtering techniques.

DGPS [3] uses a reference station at a known position to determine corrections that other local GPS receivers (within 50 km of the reference station) can use to reduce the effects of GPS common mode error sources. The extent to which the common mode errors are reduced depends on the quality of the design of the reference station. Therefore, the quality of the reference station affects the positioning accuracy that end users are ultimately able to achieve. The RTCM 104 standard [1] for DGPS corrections makes the following recommendations.

1) The range and range rate corrections be the best available estimates at the instant identified by the time tag. They should not be predicted forward in time.

Manuscript received August 3, 1998. Recommended by Associate Editor, R. Middleton. This work was prepared in cooperation with the State of California, Business, Transportation and Housing Agency, Department of Transportation, and Partners for Advance Transit and Highways (PATH).

J. Farrell is with the Department of Electrical Engineering, University of California, Riverside, CA 92505 USA (e-mail: farrell@ee.ucr.edu).

T. Givargis is with the Department of Computer Science, University of California, Riverside, CA 92505 USA (e-mail: givargis@cs.ucr.edu).

Publisher Item Identifier S 1063-6536(00)03192-4.

2) A reference station should not attempt to remove the effects of ionospheric error from the broadcast corrections.
3) A reference station should not attempt to remove the effects of tropospheric error from the broadcast corrections.
4) Except for time transfer applications, the effect of reference station receiver clock errors should be removed from the broadcast corrections.
5) The effect of satellite clock errors (based on the standard polynomial correction [4], [6]) should be removed from broadcast corrections.
6) The pseudorange measurements should be simultaneous.
7) The reference station antenna should be located and the corrections processed to minimize the effects of multipath.

The specifications of the RTCM 104 standard will serve as a basis for the design and discussion of this paper.

Ionospheric errors are not removed by the reference station, so that corrections are independent of the any particular ionospheric model. If necessary, distant users can use the best available ionospheric model to correct both the correction and their measured range for the ionospheric error at the respective locations of the reference station and user. Tropospheric errors are not removed as the errors are altitude dependent. If the user and reference station are at different altitudes, the user can correct both the correction and the measured range for the tropospheric error at the respective locations of the reference station and user.

Reference station clock bias is removed to decrease the dynamic range of the broadcast corrections and to ensure the continuity of the corrections. Similarly, the calculated satellite clock errors are removed by the reference station to decrease the dynamic range of the corrections.

The reference antenna can be carefully sited or augmented with additional hardware (e.g., choke ring) to decrease the effects of multipath; however, some multipath error will remain.

This article presents and analyzes the performance of two new algorithms for DGPS reference station implementation. The main objectives in the design of these new algorithms is the removal of noncommon mode errors (i.e., multipath and receiver noise) from the differential corrections. Theoretical and experimental data analysis are included. Existing reference station algorithms [8], [11], [13] are reviewed in Section II-D. Algorithms for determining phase corrections are not discussed. Phase correction calculation algorithms are discussed, for example, in [1] and [4]. This article does not address the important issues related to reference station integrity monitoring. Discussion of such issues can be found, for example in [3], [11], and [12]. In the remainder of this article, it will be assumed that all measurements are made simultaneously. This assumption may not be applicable to early generation receivers.

II. Background

This section presents background information necessary for reference station algorithm design and analysis. Section II-A discusses three GPS receiver measurements and their error models. Section II-B discusses the calculation of basic DGPS corrections. Section II-C discusses the calculation of a filtered reference station clock error correction. Section II-D reviews reference station algorithms that the authors were aware of at the time this article was written.

Throughout this article the notations x, $\hat{x}$, and $\tilde{x}$ will be used to denote the actual, computed, and measured values of a variable x, respectively.

A. Observables

The code pseudorange measured by a user receiver can be accurately modeled as [2], [4]

$$\begin{aligned}\tilde{\rho} = &((\hat{x}_{sv}-x)^2+(\hat{y}_{sv}-y)^2+(\hat{z}_{sv}-z)^2)^{0.5}\\ &+c\Delta t_r(t)+MP(t)+\eta(t)+c\Delta t_{sv}(t)\\ &+SA(t)+E(t)+c\Delta t_{ion}(t)+c\Delta t_{tr}(t)\end{aligned} \tag{1}$$

where

c	speed of light;
$\Delta t_r(t)$	receiver clock bias;
Δt_{sv}	satellite clock bias;
$SA(t)$	selective availability error;
$E(t)$	error in the calculated ephemeris;
$\Delta t_{ion}(t)$	dispersive ionospheric errors;
$\Delta t_{tr}(t)$	nondispersive atmospheric errors;
$MP(t)$	multipath error;
$\eta(t)$	random measurement noise.

The satellite position $(\hat{x}_{sv}, \hat{y}_{sv}, \hat{z}_{sv})$ is calculated based on the standard GPS equations [6]. The last five terms in (1) represent the common mode errors. They are referred to as common mode, since they affect all receivers in a limited geographic area in the same manner.

The objective of the DGPS reference station is to accurately estimate and broadcast real-time corrections that enable a GPS user to eliminate the effects of the common mode errors from the positioning solution. The extent to which this objective is achieved will depend on the ability of the reference station to separate the common mode and noncommon mode errors. Carrier phase information, as discussed in the next two paragraphs, can be used advantageously in this separation process.

The full carrier phase measured by a user receiver can be accurately modeled as [2], [4]

$$\begin{aligned}\tilde{\phi}\lambda = &((\hat{x}_{sv}-x)^2+(\hat{y}_{sv}-y)^2+(\hat{z}_{sv}-z)^2)^{0.5}\\ &+c\Delta t_r(t)+mp(t)+\zeta(t)+N\lambda+c\Delta t_{sv}(t)\\ &+SA(t)+E(t)-c\Delta t_{ion}(t)+c\Delta t_{tr}(t)\end{aligned} \tag{2}$$

where

$\lambda = c/f$	wavelength corresponding to the carrier frequency f;
mp	phase multipath;
ζ	phase measurement noise.

Phase multipath error has a typical magnitude on the order of a centimeter. Phase measurement noise has a standard deviation on the order of a millimeter (i.e., 1% of the wavelength). The variable N is a constant integer that represents the whole number of carrier cycles between the satellite and receiver at an initial measurement time. This integer bias is unknown. The full carrier phase measurement cannot be used as a pseudorange measurement unless the integer bias N is determined [7]. The

bias N is referred to in the GPS literature as the *integer ambiguity*.

The measured Doppler is formed as the change in the observed carrier phase over a short interval of time. The Doppler measurement can be accurately modeled as

$$\begin{aligned}\tilde{D} = &\frac{d}{dt}((\hat{x}_{sv}-x)^2+(\hat{y}_{sv}-y)^2+(\hat{z}_{sv}-z)^2)^{0.5}\\ &+\frac{d}{dt}c\Delta t_r(t)+\frac{d}{dt}mp(t)+\beta(t)+\frac{d}{dt}\\ &\cdot[c\Delta t_{sv}(t)+SA(t)+E(t)-c\Delta t_{ion}(t)+c\Delta t_{tr}(t)].\end{aligned} \tag{3}$$

Note that the Doppler measurement is not affected by the integer ambiguity, since this constant is eliminated in the time differentiation. Since all the error terms are slowly varying quantities, the Doppler measurements from four satellites can be used to provide an accurate estimate of user velocity.

For the analysis that follows, it is important to note that the dispersive ionospheric effects affect the code and phase measurements in opposite senses (i.e., code is delayed while phase is advanced [7]). The ionospheric effects are dependent on the carrier frequency and can be modeled to first order as

$$c\Delta t_{ion}(t) = \frac{A}{f^2}TEC \tag{4}$$

where TEC is the total electron count in a fixed cross sectional area along the actual path traversed by the signal between the satellite and receiver. The GPS system currently uses two carrier frequencies ($f_1 = 1575.42$ MHz and $f_2 = 1227.60$ MHz). Therefore, it is convenient for the analysis that follows to define the quantity $I_a = (A/f_1 f_2)TEC$. With this definition, the ionospheric delay affecting the pseudorange measurements derived from the f_1 and f_2 carrier signals can be represented, respectively, as

$$c\Delta t_{ion_1}(t) = \frac{f_2}{f_1}I_a \quad \text{and} \quad c\Delta t_{ion_2}(t) = \frac{f_1}{f_2}I_a. \tag{5}$$

B. Differential Corrections

A reference receiver at an accurately calibrated location (x_o, y_o, z_o) can calculate the reference-to-satellite range as

$$\hat{R}_o = ((\hat{x}_{sv}-x_o)^2+(\hat{y}_{sv}-y_o)^2+(\hat{z}_{sv}-z_o)^2)^{0.5}. \tag{6}$$

The basic range space differential correction (per satellite) is determined by differencing the calculated and measured reference-to-satellite ranges

$$\begin{aligned}\hat{\Delta}_{\mathrm{DGPS}}(t) &= \hat{R}_o - \tilde{\rho} &(7)\\ &= -(c\Delta t_o(t)+c\Delta t_{sv}(t)+SA(t)+E(t)\\ &\quad +c\Delta t_a(t)+MP(t)+\eta(t)) &(8)\end{aligned}$$

where Δt_o represents the bias in the reference receiver clock. The sign of $\Delta_{\mathrm{DGPS}}(t)$ is motivated by the RTCM DGPS standard [1] which states that the correction will be added by the remote user.

Based on the RTCM specification list, the broadcast corrections should be corrected to remove the reference receiver and satellite clock errors. Therefore, the broadcast corrections will take the form

$$\hat{\Delta}_{\mathrm{GPS}}(t) = \hat{R}_o + c\Delta\hat{t}_o(t) + c\Delta\hat{t}_{sv}(t) - \tilde{\rho} \tag{9}$$

$$\begin{aligned}&= -(c\delta t_o(t)+c\delta t_{sv}(t)+SA(t)+E(t)\\ &\quad +c\Delta t_a(t)+MP(t)+\eta(t))\end{aligned} \tag{10}$$

where $c\delta t_o$ and $c\delta t_{sv}$ represent the residual reference receiver and satellite clock errors. The residual satellite clock error is small and common to all receivers using the same set of ephemeris data to calculate the satellite clock corrections. Therefore it will be removed through differential operation. Removal of satellite clock errors prior to broadcasting the corrections greatly decreases the magnitude of the broadcast corrections without sacrificing any accuracy. The calculation of $c\Delta\hat{t}_o$ will be addressed in Section II-C.

Equation (9) shows the actual reference station calculation. Equation (10) shows the remaining error sources in the calculated signal. Note that the Δ_{DGPS} signal contains the desired common mode error sources, which will cancel the corresponding errors in the user's position calculation. It also contains the multipath and measurement noise terms. Since these errors can be as large as several meters, it is beneficial to filter the $\hat{\Delta}_{\mathrm{GPS}}$ signal to remove the noncommon mode errors prior to broadcast. Appropriate filters will be discussed in Sections II-D, III, and IV.

Similarly, a differential Doppler correction can be calculated as

$$\hat{\Delta}_{DPLR}(t) = \frac{d}{dt}[\hat{R}_o + c\Delta\hat{t}_o(t) + c\Delta\hat{t}_{sv}(t)] - \tilde{D} \tag{11}$$

$$\begin{aligned}&= -\frac{d}{dt}[c\delta t_o(t)+c\delta t_{sv}(t)+SA(t)+E(t)-c\Delta t_a(t)]\\ &\quad -\frac{d}{dt}mp(t)-\beta(t).\end{aligned} \tag{12}$$

Again, (11) represents the calculation of the correction. Each term in (11) is either calculable or measurable at the reference station. Equation (12) shows the error terms contained in the Δ_{DPLR} signal. The Δ_{DPLR} signal (per satellite) is added by the user. This Doppler correction signal is also used as an observable in one of the existing reference station algorithms discussed in Section II-D.

C. Clock Bias Compensation

In the user position calculation, any bias common to all pseudorange measurements will only effect the accuracy of the estimated user clock bias [12, p. 476, vol. I]. Therefore, it is not necessary to remove the effects of the reference receiver clock bias from broadcast corrections. The reference clock bias is removed as a matter of convenience to conserve broadcast bandwidth and to produce continuous corrections.

The reference clock bias estimate that is removed need not be exact, since the residual reference clock bias error will be identical on all the corrections. Therefore, it will only affect the user's clock bias estimate. However, due to the fact that some

users model the clock bias as a continuous time Markov process [2, Sec. 10.4], the subtracted estimate of the reference clock bias should be a very low bandwidth signal.

One method of removing clock bias at the reference station is to estimate it as the least squares estimate over all satellites available at the reference station [11], [13]

$$c\Delta\hat{t}_o = -\frac{1}{M}\left(\sum_{i=1}^{M}\left(\hat{R}_o^{(i)}(t) + c\Delta\hat{t}_{sv}^{(i)}(t) - \tilde{\rho}_o^{(i)}(t)\right)\right) \quad (13)$$

where M is the number of satellites available and the notation $(\zeta)^{(i)}$ refers the quantity ζ to the ith satellite. An alternative approach is to select $c\Delta\hat{t}_o$ to minimize the magnitude of the maximum correction. For a fixed set of satellites, the clock estimate of (13) has a smoother derivative than the estimate that would be selected to minimize the maximum magnitude.

When a new satellite becomes available or a satellite drops out, $c\Delta\hat{t}_o$ will change discontinuously by the satellite differential range correction of (9) divided by M. Such rapid changes in $c\Delta\hat{t}_o$ may affect user position accuracy depending on the implemented user algorithm. If the user algorithm involves double differencing [4], then user position will be unaffected, since all reference receiver and rover clock bias effects are removed. If the user algorithm involves single differences and the positioning algorithm involves clock model filter states, then the reference station designer must carefully consider the rate of change of $c\Delta\hat{t}_o$. When a user navigation algorithm is Kalman filter based and includes a clock model, the rate of change (i.e., bandwidth) of the clock error states is determined by the covariance of the clock state driving noise, the differential equation for the clock model, and the measurement error covariance. If the rate of change of $c\Delta\hat{t}_o$ is greater than the rate of change expected based on the clock error model, then the user position accuracy will be affected.

Due to the constraint that $c\Delta\hat{t}_o$ be very slowly time varying, the estimate of (13) should be filtered prior to adding it to the corrections. An appropriate filter could be a Kalman filter incorporating the state transition matrix and process noise covariance described in [2, Ch. 10] with $\boldsymbol{H} = [1,\ 0]$ and $R \gg 30^2/M$. The clock bias output by this filter [denoted $c\Delta\hat{t}_{of}(t)$] may still be biased, since all the error processes have not been completely modeled; however, the bias that appears in the resulting corrections will vary slowly enough that the user filter will be able to model the bias as user clock error.

The block diagram for a basic reference station is shown in Fig. 1. The figure incorporates the principles described above to produce range corrections for each in-view satellite which are corrected for satellite clock error and filtered reference station clock bias. The resultant differential corrections from this basic algorithm are those of (9). The corrections are corrupted by the reference station multipath and receiver noise. Algorithms to attenuate the effects of these noncommon mode errors on the broadcast corrections are the topic of the remainder of this article.

D. Existing Algorithms

Differential reference station algorithms have been previously presented in [11] and [13]. Both reference station

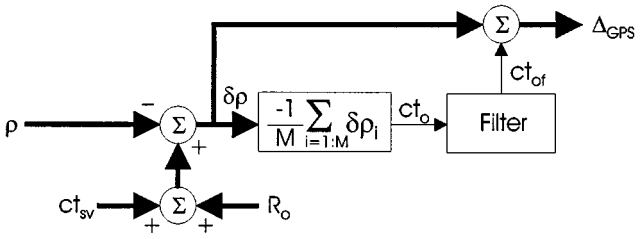

Fig. 1. Basic reference station with reference station clock bias correction. Reference (9). Wide lines represent vector variables.

algorithms can be represented by the block diagram of Fig. 2, which shows the basic DGPS corrections of Fig. 1 being filtered before they are broadcast to users. The purpose of the filtering is to reduce the noncommon mode multipath error and receiver measurement noise prior to broadcast. In addition, the filters generate the rate of change of the correction which is useful for correcting Doppler measurements and for propagating latent corrections to the time of applicability [1].

The existing algorithms and those proposed in subsequent sections are distinguished from each other by the filter model and the measurements that the filter incorporates. All the proposed filters are designed using the Kalman filtering methodology [2]. In Fig. 2, wide lines represent vector variables. For example, the wide line entering the stack of Kalman filters represents the vector of basic DGPS corrections from (9). The dimension of the vector is equal to the number of in-view satellites. The basic correction for each in-view satellite will be processed by its own Kalman filter. Subsequent text will discuss the design of this (per satellite) Kalman filter.

For the Kalman filter descriptions, the state model will be represented as

$$\boldsymbol{x}(k+1) = \boldsymbol{\Phi}\boldsymbol{x}(k) + \boldsymbol{\Gamma}\boldsymbol{\omega}(k) \quad \boldsymbol{y}(k) = \boldsymbol{H}\boldsymbol{x}(k) + \boldsymbol{\nu}(k). \quad (14)$$

Estimated variables will be indicated by hats (i.e., $\hat{\boldsymbol{x}}$). The sampling period will be denoted by T, so that $\boldsymbol{x}(k)$ denotes the kth sample of the continuous time process $\boldsymbol{x}(t)$ at the time $t = kT$.

The algorithm of [13] calculates reference station corrections by passing the basic correction of (9) through a three state Kalman filter with $\boldsymbol{x} = [c,\ v,\ a]$ where c is the filtered correction (i.e., pseudorange error), v is the rate of change of the correction, a is the acceleration of the correction. The Kalman filter is driven by the basic differential correction of (9). Therefore, the state-space model of the filter is parameterized by

$$\boldsymbol{\Phi} = \begin{bmatrix} 1 & T & \dfrac{T^2}{2} \\ 0 & 1 & T \\ 0 & 0 & 1 \end{bmatrix} \quad \text{and} \quad \boldsymbol{H} = [1,\ 0,\ 0]. \quad (15)$$

The resulting filter is suboptimal, since it neglects the time correlation in the multipath errors, which have been modeled as measurement noise. Specific values of the covariance of the discrete time driving noise and of the measurement noise are not presented in [13]. The article does state that the filter is tuned to eliminate receiver noise as much as possible without jeopardizing the ability of the filter to track the changes in the correc-

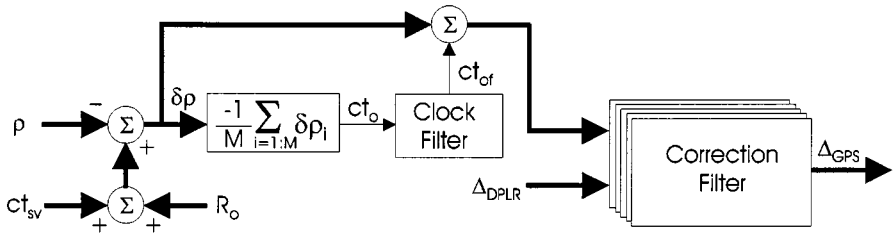

Fig. 2. Reference station design with correction filtering. Wide lines represent vector variables.

tions due to selective availability. The article shows that the difference between the corrections of two reference stations using separate antennae but identically software had standard deviations of approximately 3.6 m and peak values of approximately 10 m. Therefore, the standard deviation of a single reference station using the design of [13] would be about 2.5 m.

The algorithm of [11][1] is based on a four state filter $\boldsymbol{x} = [c,\ v,\ a,\ e]^T$ where c, v, and a are as defined above, and e represents the difference between the rates of change of the code and carrier pseudorange corrections. This fourth state is used to allow the filter to account for the fact that changes in the ionospheric error affect the code and phase measurements in opposite senses. The state transition model is parameterized by

$$\boldsymbol{\Phi} = \begin{bmatrix} 1 & T & \dfrac{T^2}{2} & 0 \\ 0 & 1 & T & 0 \\ 0 & 0 & 1 & 0 \\ 0 & 0 & 0 & 1 \end{bmatrix}. \tag{16}$$

The covariance of the discrete time driving noise is discussed, but not completely specified in [11]. The driving noise spectral densities were tuned to achieve the objectives of: 1) the fourth state having low enough bandwidth to accumulate the ionospheric divergence between the code and carrier measurements, while remaining unaffected by the code multipath and 2) the first three states accurately reflecting the common mode errors, while being unaffected by noncommon mode errors. The filter uses the measurements of (9) and (11) as observables. Therefore, the observation matrix is

$$\boldsymbol{H} = \begin{bmatrix} 1 & 0 & 0 & 0 \\ 0 & 1 & 0 & -2 \end{bmatrix}. \tag{17}$$

The standard deviation of the range and Doppler correction measurements were defined to be $\sigma_\eta \in [1, 2]$ m and $\sigma_\beta = 0.01(m/s)$. This algorithm does not model the code multipath as a separate state, instead including the code multipath in the η term. Therefore, the η term has significant time correlation violating the standard Kalman filter assumptions. Article [11] also discussed issues related to integrity management, filter health, and data reasonableness checking. These issues will not be discussed herein. Hatch filtering [7] is another means by which the carrier pseudorange can be used to smooth the code-based range corrections. Unfortunately, this method can lead to "code carrier divergence" as discussed in [11], which was a primary motivation for the approach described above from [11].

The filter presented in [13] is able to decrease the effect of the high frequency random receiver noise, but cannot substantially decrease the effects of multipath since the frequency content of the corrections and the multipath error are very similar. Both have correlation times on the order of minutes. The filter presented in [11] uses Doppler measurements to smooth the code corrections. This requires one additional state, but gives the filter a greater ability to reject multipath errors. Performance statistics are not presented in [11], but can be inferred (using a PDOP[2] ≈ 3) to be at the 1.6–2.6 m level based on the 5–8 m position accuracies stated in the conclusion of that article.

An alternative two frequency reference station algorithm is presented in [8].[3] Distinctions between [8] and this article include: the algorithm herein uses eight physical states while the algorithm of [8] uses 11 nonphysical states; the presentation of this article includes a thorough theoretical analysis; and, the experimental analysis of the present article allows a more complete understanding of the accuracy of the reference station DGPS corrections. Due to space limitations, a comprehensive presentation of the method of [8] has not been included herein.

The subsequent sections of this article will present a six state single frequency reference station filter and an eight state two frequency reference station filter. Each filter will utilize both code and phase pseudorange measurements. Each filter will be analyzed both analytically and experimentally to determine the filter performance. The main objective being to generate corrections essentially free of the effects of code multipath and measurement noise.

III. Single Frequency Reference Station Design

This section presents a theoretical analysis of the performance of a single frequency reference station algorithm driven by code and phase pseudorange measurements. Due to the different effect that ionospheric effects have on the two measurements, the ionospheric effects will need to be modeled separately from the remaining forms of common mode error. For this purpose, let the desired differential correction for the f_1 code pseudorange be

$$\Delta_{\mathrm{DGPS}} = -r_c - \frac{f_2}{f_1} I_a \tag{18}$$

[1]The following description is slightly modified from that presented in the cited article to show the consistency and distinction of the approach relative to the subsequent approaches and to account for changes in receiver technology since the time the cited article was written. The modifications are minor and most were alluded to within the cited paper.

[2]Position dilution of position is an approximate multiplicative factor relating the range and position error standard deviations [2], [4], [12].

[3]The authors thank the reviewers for alerting them to the existence of [8].

where I_a was defined in (5) and

$$r_c(t) = c\delta t_o(t) + c\delta t_{sv}(t) + SA(t) + E(t). \tag{19}$$

Since the differential correction calculated at the reference station is corrupted by multipath and receiver noise, the measured correction is modeled as

$$\Delta_{\mathrm{DGPS}} = -r_c - \frac{f_2}{f_1} I_a - MP - \eta. \tag{20}$$

Let $z_1 = \Delta_{\mathrm{DGPS}}$ (measured in meters), then

$$\tilde{z}_1(t) = \hat{R}_o(t) + c\Delta\hat{t}_{sv}(t) + c\Delta t_{of} - \tilde{\rho}_{o1}(t) \tag{21}$$

$$= -r_c - \frac{f_2}{f_1} I_a - MP_1 - \eta_1. \tag{22}$$

Let z_2 denote a similarly processed version of the measured f_1 carrier phase range correction (measured in cycles) at the reference station, then

$$\tilde{z}_2(t) = (\hat{R}_o(t) + c\Delta\hat{t}_{sv}(t) + c\Delta t_{of})/\lambda_1 - \tilde{\phi}_{o1}(t) \tag{23}$$

$$= \frac{-1}{\lambda_1} r_c + \frac{1}{\lambda_2} I_a - N_1 - mp_1 - \nu_1 \tag{24}$$

where the subscripts in the right-hand side of the equation indicate to which carrier frequency the subscripted variable refers.

Use of both the code and phase measurements to drive the filter will therefore require the state to be defined as $\boldsymbol{x} = [r_c, \dot{r}_c, \ddot{r}_c, MP, I_a, N]^T$. The first three state variables represent the range correction and its first two derivatives, excluding ionospheric effects. The fourth state represents code multipath, which is to be removed. The fifth state represents ionospheric effects, which are modeled separately to properly account for their different effects on the code and carrier observables. The sixth state accounts for the carrier integer ambiguity, which will be estimated as a real variable. The measurement matrices corresponding to the two observable variables z_1 and z_2 are

$$z_1(t) = \boldsymbol{H}_1 \boldsymbol{x}, \qquad \boldsymbol{H}_1 = \left[-1, 0, 0, -1, -\frac{f_2}{f_1}, 0\right] \tag{25}$$

$$z_2(t) = \boldsymbol{H}_2 \boldsymbol{x}, \qquad \boldsymbol{H}_2 = \left[\frac{-1}{\lambda_1}, 0, 0, 0, \frac{1}{\lambda_2}, -1\right]. \tag{26}$$

The desired differential correction outputs can be calculated from the filter state as

$$y_1(t) = \boldsymbol{L}_1 \boldsymbol{x}(t), \qquad \boldsymbol{L}_1 = \left[-1, 0, 0, 0, -\frac{f_2}{f_1}, 0\right] \tag{27}$$

$$y_2(t) = \boldsymbol{L}_2 \boldsymbol{x}(t), \qquad \boldsymbol{L}_2 = [0, -1, 0, 0, 0, 0]. \tag{28}$$

The output y_1 represents the range correction including ionospheric error, but processed to remove multipath, code measurement noise, reference station clock error, and predicted space vehicle clock error. The output y_2 represents the range correction rate of change.

To construct the state-space differential equation, the first three states use a PVA (position, velocity, acceleration) model [2], the multipath and ionospheric states are modeled as first-order Markov processes, and the integer ambiguity is modeled as a random constant. The state-space model is therefore

$$\dot{\boldsymbol{x}}(t) = \begin{bmatrix} 0 & 1 & 0 & 0 & 0 & 0 \\ 0 & 0 & 1 & 0 & 0 & 0 \\ 0 & 0 & -\frac{1}{\tau_a} & 0 & 0 & 0 \\ 0 & 0 & 0 & -\frac{1}{\tau_M} & 0 & 0 \\ 0 & 0 & 0 & 0 & -\frac{1}{\tau_i} & 0 \\ 0 & 0 & 0 & 0 & 0 & 0 \end{bmatrix} \boldsymbol{x}(t) + \boldsymbol{\omega}(t) \tag{29}$$

where τ_a are τ_M are on the order of minutes and τ_i is on the order of hours. These correlation times are selected on the basis of the physics behind the processes and the experimental results reported in the literature [4], [9], [12]. For the simulations and experiments that follow, $\tau_a = 60$ s, $\tau_M = 300$ s, and $\tau_i = 21\,600$ s.

The spectral density of the white driving noise vector (i.e., $\boldsymbol{Q}_\omega$) was selected so that the magnitude of the steady state covariances in a simulation without GPS measurements would match the magnitude of the covariance of the physical process. Calculation of the steady-state covariance is described for example in [4, Sec. 3.4.4]. Letting the covariances of the (uncorrected) acceleration, multipath, and ionospheric states be denoted by P_a, P_M, and P_i, respectively, $\mathrm{diag}(\boldsymbol{Q}_\omega) = 2[0, 0, P_a/\tau_a, P_M/\tau_M, P_i/\tau_i, 0]$. For the results that follow, $P_a = 1 \times 10^{-4}(m/s^2)^2$ and $P_i = 100.0$ m^2. Performance will be evaluated for various levels of multipath (i.e., values of P_M).

Fig. 3 shows in block diagram form the implementation of the single frequency reference station that incorporates filtering to reduce the effects of code multipath and measurement noise. Note that the clock bias estimation portion of the implementation is identical to that of Fig. 1.

A observability analysis of (29) with measurements described by (25) and (26) shows that the state vector is observable from the measurements; however, the condition number of the observability matrix is very high (10^9). Physically, the state is observable, but the time required to accurately estimate the states might be prohibitively long. The first three states reflect quantities affecting both measurements. The multipath state affects only the code pseudorange estimate. Although multipath error also effects the carrier phase measurements, the magnitude of the phase multipath error is much smaller than the code multipath error and has been neglected. The ionospheric state affects both measurements, but in opposite directions. The integer ambiguity state affects only the phase measurement. Due to the different linear combinations, the state is theoretically observable; however, due to the very long time constants, separation of the multipath, ionospheric, and integer ambiguity states may require long periods of time. Fortunately, complete separation of these states is not required to accurately estimate the desired

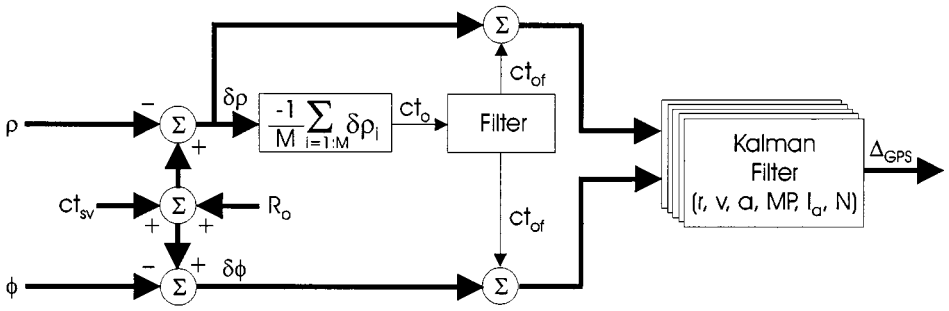

Fig. 3. Single frequency reference station design with correction filtering. Wide lines represent vector variables where $v = \dot{r}$ and $a = \ddot{r}$.

range correction of (27). A covariance analysis is required to more thoroughly analyze the expected performance of the proposed base station algorithm.

Fig. 4 shows the results of a covariance analysis for a single frequency reference station. These figures were generated by propagating the Kalman filter covariance equations under the following assumptions. Single frequency code and phase measurements were processed at a 1.0-Hz rate for 160 min. The covariance of the corrections reaches its steady-state value within about 15 min, so only the first 30 min of results are plotted. The measurement noise standard deviations were 0.5 m. for code measurements and 0.01 cycles for phase measurements. These are typical values for receivers. More expensive receivers would result in smaller errors, especially in the code measurements.

The five different plots in each figure correspond to the results of five different covariance analysis simulations. Each simulation used a different power spectral density for the code multipath driving noise. From bottom to top on each figure the plots correspond to steady-state (uncorrected) multipath errors with standard deviations of 0.1, 0.5, 1.0, 2.0, and 3.0 m. These plots corresponding to different multipath scenarios are included to allow the reader to evaluate the utility of improving the reference station hardware (e.g., choke ring antenna, higher fidelity receiver).[4]

The seven figures illustrate the estimation error standard deviation of the six filter states [i.e., Fig. 4(a)–(e)] and the range correction [i.e., Fig. 4(f)]. The figures clearly show the benefits of carefully choosing antenna technologies (e.g., ground plane, choke ring) and antenna location to minimize the received multipath. Careful comparison between error standard deviation plots for the filter states (i.e., r_c, N, and I_a) and for the corrections shows that although the filter cannot accurately estimate each of the variables in the former set of plots individually, the filter is able to accurately estimate the correction to essentially the same level of accuracy as the multipath. Presumably this is due to the carrier smoothing of the code signal. The covariance simulations predict correction covariances between 0.5 and 2.5 m. depending on the level of multipath. Note that this is similar performance to that inferred for the method of [11] in Section II-D. Neither method is able to accurately estimate, and hence substantially reduce the effects of, the multipath error. Both methods essentially use the phase information to smooth the code measurement. The state-space model proposed herein is more complete, which allows for improved performance but also requires increased computation.

Note from the velocity and acceleration error standard deviation plots [i.e., Fig. 4(b)] that within 12 s, the rate and acceleration estimation errors have reached steady-state accuracy. Accurate estimation of the rate and acceleration is due to these two states being observable from changes in the phase, which are independent of the integer ambiguity N. The range correction reaches steady-state accuracy in 15 min as does the multipath estimation error. The first state, ionospheric estimate, and ambiguity estimate have still not reached steady state at the end of the simulation. This last issue is somewhat immaterial, as long as the correction error is in steady state.

Even after the 160 min the ionosphere, integer, and first state error standard deviations have not reached steady state. At 160 min, one standard deviation error in the integer ambiguity would still allow ≈140 integer values. The objective is not to identify this ambiguity, but to properly model the effect of this large constant bias on the phase measurement.

Experimental results for this reference station algorithm are presented in Section V.

IV. Two Frequency Reference Station Design

To more accurately account for atmospheric errors and hence obtain better observability of the multipath errors, a two frequency reference station can be designed. Again, the filter defined below is for a single satellite. Identical, but independent, filters would be implemented for each satellite in view of the base. The architecture of the algorithm is similar to that shown in Fig. 3, except for the differences in the observables and state vector definition as described below.

With a two frequency receiver, four observable variables based on the two frequency pseudorange and phase measurements will be used. The measurements corresponding to f_1 are defined in (22)–(24). The measurements corresponding to f_2 are

$$\tilde{z}_3 = \hat{R}_o(t) + c\Delta\hat{t}_{sv}(t) + c\Delta\hat{t}_{of} - \tilde{\rho}_{o2}(t) \tag{30}$$

$$= -r_c(t) - MP_2(t) - \frac{f_1}{f_2} I_a - \eta_2 \tag{31}$$

[4]Note that the results presented herein have assumed constant parameters for the multipath dynamic model. In fact, the multipath model parameters are elevation dependent. Since satellite elevation is calculable at the base station, this dependence could be built in to the algorithm. Such modifications would only improve the demonstrated experimental performance.

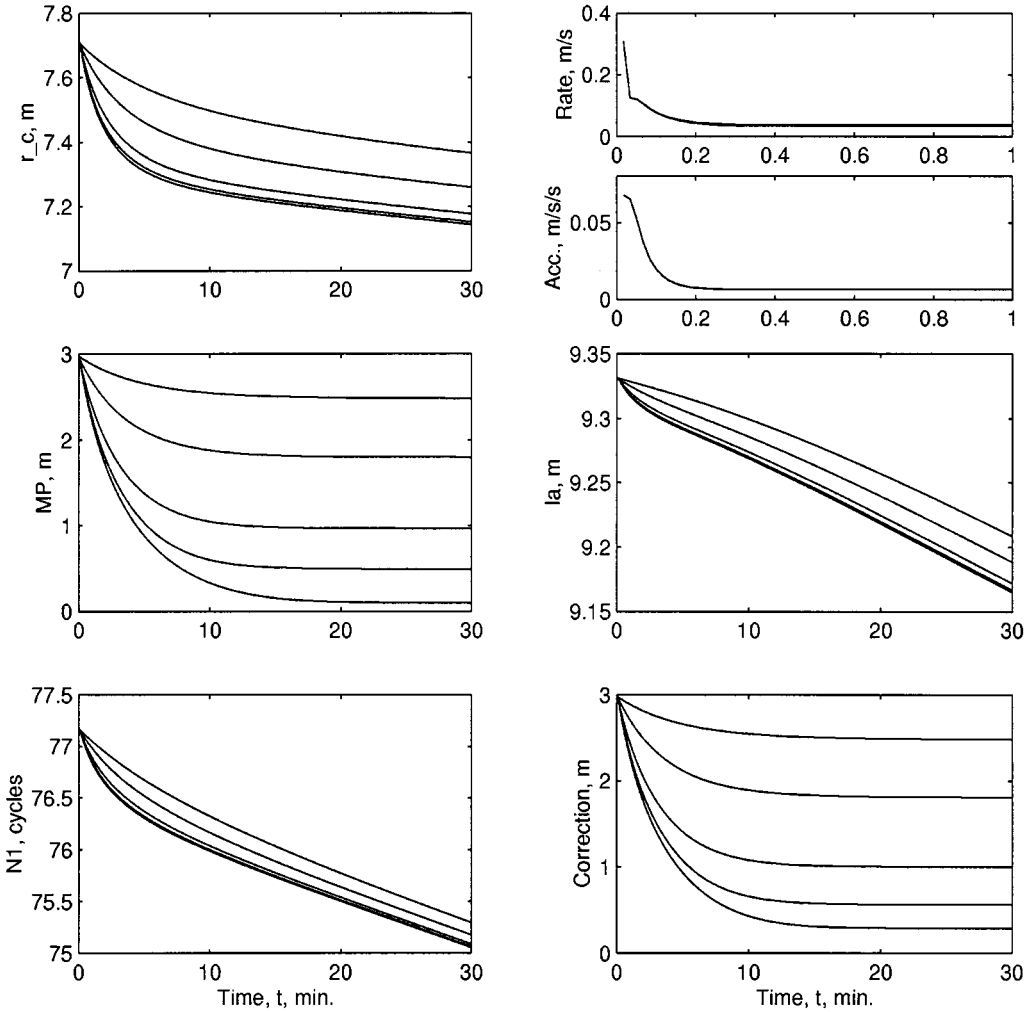

Fig. 4. Theoretical performance results for the single frequency reference station. The five plots in each subfigure correspond (bottom to top) to actual multipath error standard deviations of 0.1, 0.5, 1.0, 2.0, and 3.0 m: (a) top left—standard deviation of the estimated common mode errors excluding ionospheric effects, (b) top right—Standard deviation of the estimated rate and acceleration of the range correction, (c) middle left—standard deviation of the estimated multipath error, (d) middle right—standard deviation of the estimated ionospheric error, (e) bottom left—standard deviation of the estimated L1 integer ambiguity, and (f) bottom right—standard deviation of the estimated range correction.

$$\tilde{z}_4 = (\hat{R}_o(t) + c\Delta\hat{t}_{sv}(t) + c\Delta\hat{t}_{of})/\lambda_2 - \tilde{\phi}_{o2}(t) \quad (32)$$

$$= \frac{-1}{\lambda_2} r_c(t) + \frac{1}{\lambda_1} I_a - N_2 - \nu_2. \quad (33)$$

Two additional states are required, relative to the one frequency reference station, to model the integer ambiguity and multipath errors on the second carrier frequency. The state is then defined to be

$$\boldsymbol{x} = [r_c, \dot{r}_c, \ddot{r}_c, MP_1, MP_2, I_a, N_1, N_2]^T.$$

The dynamic and driving noise models for the two new states are the same as the corresponding states in the single frequency model.

The measurement matrices for the two f_2 observable variables are

$$z_3 = \boldsymbol{H}_3\boldsymbol{x}, \qquad \boldsymbol{H}_3 = \left[-1, 0, 0, 0, -1, -\frac{f_1}{f_2}, 0, 0\right] \quad (34)$$

and

$$z_4 = \boldsymbol{H}_4\boldsymbol{x}, \qquad \boldsymbol{H}_4 = \left[-\frac{1}{\lambda_2}, 0, 0, 0, 0, \frac{1}{\lambda_1}, 0, -1\right]. \quad (35)$$

The desired outputs are

$$y_1 = \boldsymbol{L}_1\boldsymbol{x}, \qquad \boldsymbol{L}_1 = \left[-1, 0, 0, 0, 0, -\frac{f_2}{f_1}, 0, 0\right] \quad (36)$$

$$y_2 = \boldsymbol{L}_2\boldsymbol{x}, \qquad \boldsymbol{L}_2 = [0, -1, 0, 0, 0, 0, 0, 0] \quad (37)$$

The output y_1 is the f_1 range corrections including atmospheric error, but processed to remove multipath, code measurement noise, reference station clock error, and predicted space vehicle clock error. The output y_2 represents the range correction rate of change. The rate correction neglects $\dot{I}_a$ since it is typically small (i.e., $\approx 5 \times 10^{-4} m/s$). Corrections for the f_2 signals are also straightforward to generate from the state estimates.

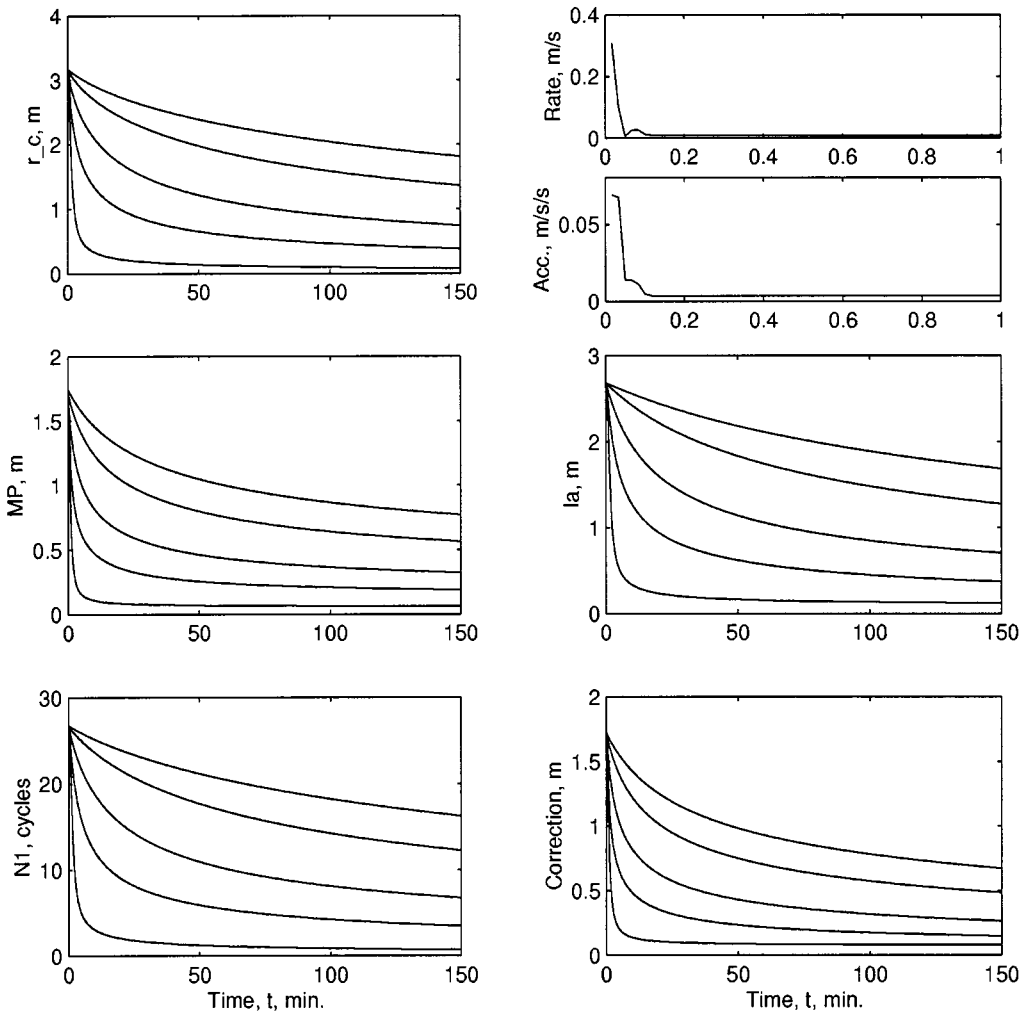

Fig. 5. Theoretical performance results for the two frequency reference station. The five plots in each subfigure correspond (bottom to top) to actual multipath error standard deviations of 0.1, 0.5, 1.0, 2.0, and 3.0 m: (a) top left—standard deviation of the estimated common mode errors excluding ionospheric effects, (b) top right—standard deviation of the estimated rate and acceleration of the range correction, (c) middle left—standard deviation of the estimated multipath error, (d) middle right—standard deviation of the estimated ionospheric error, (e) bottom left—standard deviation of the estimated L1 integer ambiguity, and (f) bottom right—standard deviation of the estimated range correction.

The state-space model is

$$\dot{\boldsymbol{x}} = \begin{bmatrix} 0 & 1 & 0 & 0 & 0 & 0 & 0 & 0 \\ 0 & 0 & 1 & 0 & 0 & 0 & 0 & 0 \\ 0 & 0 & -\frac{1}{\tau_a} & 0 & 0 & 0 & 0 & 0 \\ 0 & 0 & 0 & -\frac{1}{\tau_M} & 0 & 0 & 0 & 0 \\ 0 & 0 & 0 & 0 & -\frac{1}{\tau_M} & 0 & 0 & 0 \\ 0 & 0 & 0 & 0 & 0 & -\frac{1}{\tau_i} & 0 & 0 \\ 0 & 0 & 0 & 0 & 0 & 0 & 0 & 0 \\ 0 & 0 & 0 & 0 & 0 & 0 & 0 & 0 \end{bmatrix} \boldsymbol{x} + \boldsymbol{\omega} \tag{39}$$

where all the parameters and driving noise spectral densities are defined as for the single frequency reference station.

Fig. 5 shows performance plots for a covariance analysis of a two frequency reference station. These figures were generated in the same manner as Fig. 4 with the same parameter values. Again, the five different plots in each figure correspond to the results of five different simulations. Each simulation used a different level for the multipath driving noise. From bottom to top on each figure the plots correspond to steady-state (uncorrected) multipath errors with standard deviations of 0.1, 0.5, 1.0, 2.0, and 3.0 m. All the conclusions stated for the single frequency reference station concerning the ability to separately estimate the various states again apply. In addition, the steady-state standard deviations of the corrections are 2.5–3.0 times lower than those of the single frequency reference station.

Again, the rate and acceleration estimation error standard deviations converge to the cm/s and cm/s/s level within 10 s. This rapid convergence is again due to the accuracy of the phase measurements and the independence of the rate and acceleration estimates from the constant values of N_1 and N_2.

Note that the two frequency measurements yield a greater ability to accurately estimate I_a and the integers. Conceptually, z_1 and z_3 allow the estimation accuracy for I_a to be improved. This increased information about I_a allows z_1 and z_2 to more accurately estimate N_1. This improved integer accuracy allows z_2

TABLE I
VARIOUS STATISTICS RELATED TO THE REFERENCE STATION CORRECTION DIFFERENCES

	Max for $t > 0$			Max for $t > 1000$			Std. for $t > 0$			Std. for $t > 1000$		
PRN	u	1	2	u	1	2	u	1	2	u	1	2
4	2.1	1.5	1.1	2.1	1.3	.19	.57	.41	.18	.55	.38	.07
5	2.0	1.5	.99	2.0	1.2	.23	.54	.35	.12	.50	.31	.06
8	2.2	1.6	1.0	1.8	1.1	.61	.52	.35	.18	.47	.29	.12
9	2.1	1.1	.36	2.1	1.1	.16	.39	.23	.05	.39	.23	.03
24	2.0	1.3	.82	2.0	1.2	.67	.49	.34	.15	.47	.32	.12

and z_4 to be used directly to estimate r_c and MP. The Kalman algorithm keeps track of the covariances through time to allow this to proceed properly.

V. EXPERIMENTAL ANALYSIS

To experimentally determine the reference station performance, two reference stations running identical reference station software were run simultaneously. Each reference station receiver was connected to its own antenna. The antennae were located on a building roof edge approximately 5 m above the surface of the earth. The surface of the earth adjacent to the building was a large parking lot. The differential separation of the antennae is $(n, e, h) = (-3.28, -1.62, 0.29)$ m. The data presented is the difference between the corrections generated by the two reference stations. The mean of the difference (across all available satellites at both bases) at each sampling instant is also removed, as the mean will only affect the user clock estimate not the user position (see Section II-C). This is essentially the same experimental setup and procedure as described relative to [13, Fig. 8].

The hardware for each reference station includes an Ashtech Z-XII receiver and antenna, and a 486 equivalent PC. The antenna used a ground plane, but did not use a choke ring. The hardware for broadcasting the corrections does not affect this analysis. Instead, each reference station calculated and stored time stamped corrections to disk. The corrections were later analyzed and processed.

The reference station software simultaneously calculated the basic differential corrections, the single frequency corrections, and the two frequency corrections for all available satellites in real-time. Therefore, the results of the unfiltered, single frequency and two frequency filters are directly comparable and based on identical receiver measurements.

Due to space limitations, the graphical data is only presented for a single satellite (PRN 4). The experimental results for a set of five satellites are summarized in Table I. The presented data was collected the morning of June 9, 1998 for the satellites with PRN's: 4, 5, 8, 9, and 24.

Fig. 6 shows the difference between the basic unfiltered corrections. The data is stored at a 1.0-Hz rate. Therefore, the plot represents about 6000 samples. The difference between the corrections of the two bases has considerable high and low frequency variation. The low-frequency variations are attributed predominantly to multipath.

Fig. 7 shows the difference in the reference station corrections as generated by the single frequency reference station. The single frequency reference station algorithm is able to decrease the effects of receiver noise, but cannot significantly reduce the effects of multipath. Although slight improvements in performance are possible through additional filter tuning, dramatic increases in performance cannot be expected. As predicted in Fig. 4 the single frequency reference station algorithm is not able to accurately observe the ionospheric state I_a. Since this state is very slowly changing, the filter has difficulty discriminating the integer ambiguity N_1. Therefore, the phase measurement cannot be used as a pseudorange signal by the filter to directly estimate r_c. The filter instead uses the change in the phase measurement to accurately and rapidly ($t < 0.1$ min) estimate the velocity and acceleration of the correction. The single frequency reference station algorithm uses the phase measurement to smooth the corrections (i.e., accurate rate), but cannot accurately discriminate the correction from the multipath. The single frequency reference station therefore yields performance very similar to, but slightly better than, the performance that would result from a reference station filter using code pseudorange and Doppler as presented in [11]. (See the related discussion in Section III.) The algorithms proposed herein also require more computation, due to their higher state dimension, than those proposed in [11] and [13].

Fig. 8 shows the difference in the reference station corrections as generated by the two frequency reference station. After a brief ($\approx$10 min) transient period, the two frequency reference station correction difference is significantly less than that of the basic or single frequency reference station algorithms. The improved performance of the two frequency reference station algorithm is due to the increased observability of the ionospheric state I_a. The observability of I_a allows both integers to be estimated rather accurately so that the phase measurements can be used directly as pseudorange estimates in the estimation of r_c. Therefore, multipath errors can be accurately discriminated from the ionosphere and r_c states. Note that multipath errors are essentially eliminated after a 10-min transient period. This 10-min transient period corresponds well with the transient predicted via the covariance simulations.

Fig. 9 shows the correlation function of the reference station differences for the satellite with PRN 4 for time shifts of 0–300 s. The correlation functions were generated using the correction differences only for $t \geq 30$ min to ensure that the filter was operating in steady state. The correlation functions for all three reference stations are shown on the same graph. The correlation function for the two frequency reference station is difficult to distinguish from the time axis, but is relatively constant at approximately 0.01 m.

Fig. 10 shows the power spectral density of the reference station correction differences for the three reference station algorithms for frequencies between 0.001–0.5 Hz. The single frequency filtering gives a roughly 6-dB improvement over the basic unfiltered corrections at all frequencies. The two frequency filtering gives better that 20-dB improvement over the basic unfiltered corrections at all frequencies.

Table I shows statistics of the reference station correction differences for all five satellites that were available for the entire duration of the experiment (approximately 6000 s). The first column shows the satellite identity by means of its PRN. The remainder of the table is subdivided into four sets of columns. The column headings "u," "1," and "2" in each section of table

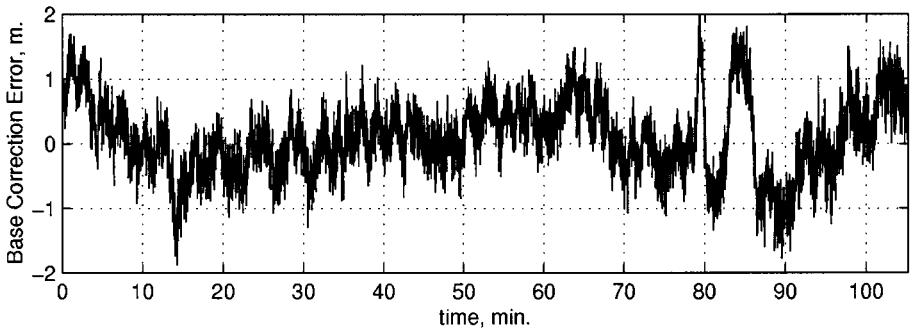

Fig. 6. Basic unfiltered reference station correction difference for PRN 4.

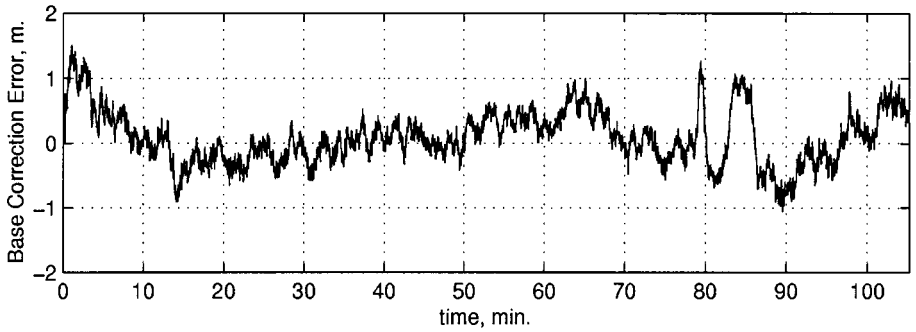

Fig. 7. Single frequency filtered reference station correction difference for PRN 4.

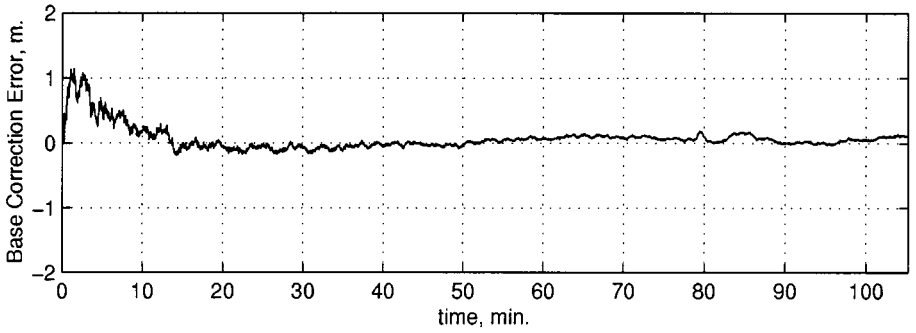

Fig. 8. Two frequency filtered reference station correction difference for PRN 4.

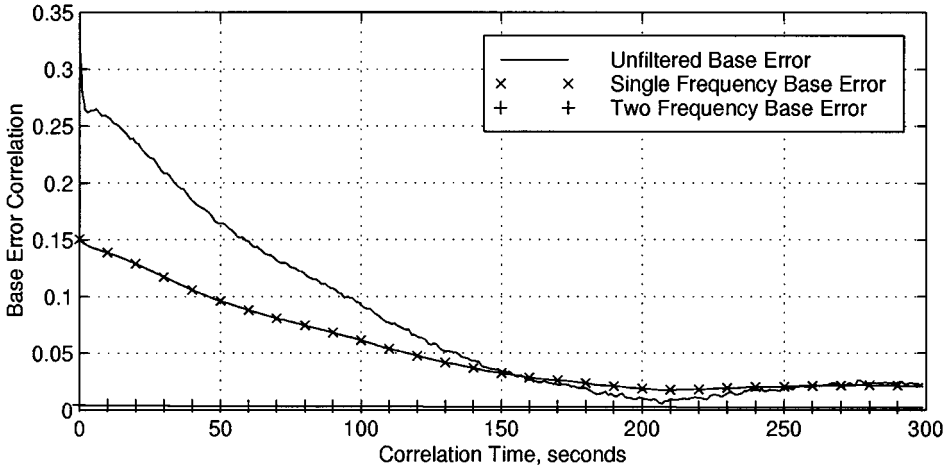

Fig. 9. Correlation functions for reference station correction differences for PRN 4 for $t \geq 30$ min.

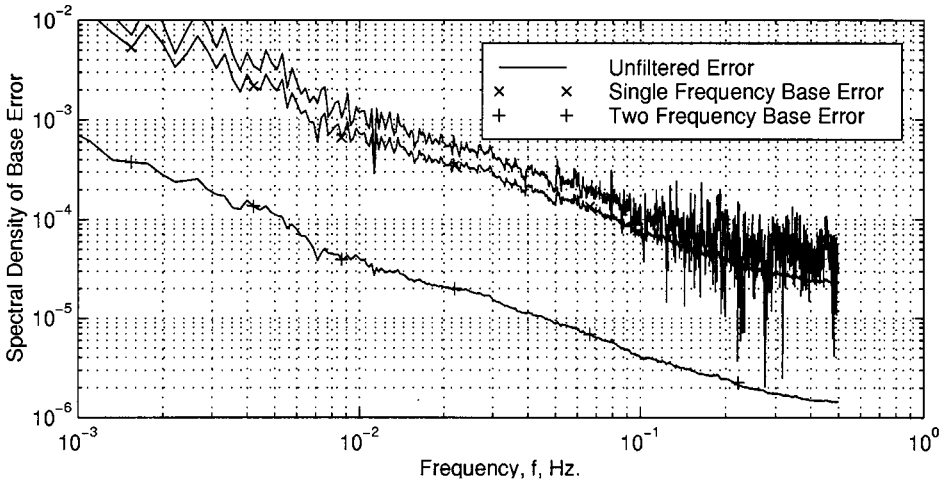

Fig. 10. Spectral density of reference correction difference for PRN 4 for $t \geq 30$ min.

indicates that the column of data is for the unfiltered, single frequency, and two frequency reference station algorithms, respectively. The four sections of the table indicate the maximum value of the correction difference and the standard deviation of the correction difference for the entire experiment and the steady state portion of the experiment. The factor of ten improvement is easily noticed in all four statistics for satellites 4, 5, and 9. For satellites 8 and 9, significant multipath error at the start of the experiment caused the correction difference to still be decaying toward zero at $t = 1000$ s. This affects both the maximum value and the standard deviation, but the effect decays steadily with time. All the data in the table is for the reference station correction differences. To estimate the standard deviation of the error for a single base, the presented standard deviation should be divided by $\sqrt{2}$. To estimate the peak error of one base, the maximum of the correction differences should be divided by two.

VI. Conclusions

This article has presented and analyzed two new algorithms for the design of reference stations for differential GPS implementations. Improvement in the performance of a DGPS reference station results in improved positioning accuracy for all users of the resulting differential corrections. The algorithms presented herein incorporate both code and phase pseudorange data for DGPS correction estimation. Both theoretical and experimental analysis is presented. The analysis shows that the single frequency reference station is not capable of accurately removing multipath errors from the broadcast corrections. Alternatively, the two frequency reference station is able to accurately estimate and remove the effects of multipath from the broadcast corrections. The single frequency and two frequency reference station algorithms improved the accuracy of the basic corrections by 6 and 20 dB, respectively. Accuracy as a function of distance from the base station has not been addressed, as this loss of accuracy is the same for all local area differential reference stations. Related issues are discussed in [12, Ch. 1, vol. II].

All DGPS reference station algorithms have some transient period. The algorithms presented herein have approximately 10-min transient periods between satellite acquisition and steady-state filter operation. This length of time corresponds to the first 1/72 of the satellite 6-h fly-by or approximately 5° of elevation change. Since most users ignore satellites below a threshold elevation of 5–10°, the reference station corrections would be in steady state before the corrections began to be used. During this low elevation portion of the fly-by, multipath errors are most significant, so the ability of the two frequency algorithm to reject multipath is critical. From an alternative point of view, even during the transient period, the two frequency algorithm outperforms the other algorithms.

The implementation of the two frequency reference station requires an eight state Kalman filter for each satellite and a single reference station clock correction filter. The calculations required for this implementation do not impose a significant computational burden for state of the art computers. In fact, the experiments presented herein implemented the clock filter and the single and the two frequency reference station Kalman filters for at least eight satellites with writing of data to the hard disk at a 1.0-Hz rate on an IBM compatible 66-MHz 486 computer. If desired, the computational load could be significantly decreased by either curve fitting the optimal filter gains or using stored gains for the steady state portion of the operation (i.e., $t > 10$ min).

References

[1] "RTCM recommended standards for differential navstar GPS service," RTCM Special Committee no. 104, Version 2.1, Jan. 3, 1994.
[2] R. Brown and Y. Hwang, *Introduction to Random Signals and Applied Kalman Filtering*, 2nd ed. New York: Wiley, 1992.
[3] P. Enge, R. Kalafus, and M. Ruane, "Differential operation of the global positioning system," *IEEE Commun. Mag.*, vol. 26, no. 7, pp. 48–60, 1988.
[4] J. Farrell and M. Barth, *The Global Positioning System and Inertial Navigation: Theory and Practice*. New York: McGraw-Hill, 1998.
[5] J. Farrell, M. Djodat, M. Barth, and M. Grewal, "Latency compensation for differential GPS," *Navigation: J. Inst. Navigation*, vol. 44, no. 1, pp. 99–107, 1997.
[6] ARINC Research Corporation, "NAVSTAR GPS Space Segment/Navigation User Interfaces, Rep. ICD-GPS-200,", Apr. 1993.
[7] R. Hatch, "The synergism of GPS code and carrier measurements," in *Proc. 3rd Int. Geodetic Symp. Sat. Doppler Pos.*, Las Cruces, NM, 1982.
[8] X.-X. Jin, "A new algorithm for generating carrier adjusted differential GPS corrections," *J. Geodesy*, vol. 70, pp. 673–680, 1996.

[9] E. Kaplan, Ed., *Understanding GPS: Principles and Applications*. Boston, MA: Artech House, 1996.
[10] T. Logsdon, *Understanding the Navstar, GPS, GIS, and IVHS*. New York: Van Nostrand Reinhold, 1995.
[11] P. Loomis, G. Kremer, and J. Reynolds, "Correction algorithms for differential GPS reference stations," *Navigation: J. Inst. Navigation*, vol. 36, no. 2, pp. 179–193, 1989.
[12] B. Parkinson, P. Axelrad, and P. Enge, Eds., *Global Positioning System: Theory and Applications*: AIAA, 1996.
[13] L. Vallot, S. Snyder, B. Schipper, N. Parker, and C. Spitzer, "Design and flight test of a differential GPS/inertial navigation system for approach/landing guidance," *Navigation: J. Inst. Navigation*, vol. 38, no. 2, pp. 321–340, 1991.

Jay Farrell (M'85–SM'98) received the B.S. degrees in physics and electrical engineering from Iowa State University, Ames, in 1986, and the M.S. and Ph.D. degrees in electrical engineering from the University of Notre Dame, Notre Dame, IN, in 1988 and 1989, respectively.

He joined the technical staff at the Charles Stark Draper Laboratory in Cambridge, MA, in 1989. While at the Draper Lab he was Principal Investigator on several projects in the areas of intelligent and learning control systems for autonomous vehicles. He joined the faculty of the College of Engineering at the University of California, Riverside in January 1994. He is currently an Associate Professor in and Chair of the Electrical Engineering Department. His current research interests include identification and on-line control for nonlinear systems, navigation, and artificial intelligence techniques for autonomous dynamic systems.

Dr. Farrell is a member of the Pi Mu Epsilon, Eta Kappa Nu, Phi Kappa Phi, and Phi Beta Kappa honorary societies. While at Iowa State he received Academic Excellence Scholarships from the Honeywell Foundation and NCR Corporation. He received the Engineering Vice President's Best Technical Publication Award in 1990, and Recognition Awards for Outstanding Performance and Achievement in 1991 and 1993. While at Notre Dame, he received a Fellowship from the Notre Dame Center for Applied Mathematics.

Tony Givargis received the B.S. degree in computer science in 1997 from the University of California, Riverside, where is currently a Ph.D. student.

His research interests include developing reusable intellectual property cores, system-on-chip design and optimizing on-chip bus structures for reduced power. In addition his research interests are hardware/software system design, embedded systems and micro-controller-based control systems.

As an under-graduate honor student, Mr. Givargis received the Betty P. Ribal Mathematics Scholarship in 1995, and the International Council on Systems Engineering Scholarship in 1997. He has also received the Outstanding Academic Program Excellence and the Student Commencement Awards from Marlan and Rosemary Bourns College of Engineering in 1997. In 1997 and 1998, respectively, he received a MICRO fellowship and the 35th Design Automation Conference Graduate Scholarship.